Editorial Summary Electrons in f orbitals can create localised states that interact strongly and drive strange metal and critical behaviour via the Kondo mechanism. Now, a mechanism of geometric frustration enables similar phenomena with d electrons.

Peer Review Information *Nature Physics* thanks William Meier and the other, anonymous, reviewers for their contribution to the peer review of this work.

Hopping frustration-induced flat band and strange metallicity in a kagome metal

Linda Ye,[1,*] Shiang Fang,[2,1] Mingu Kang,[1] Josef Kaufmann,[3,4] Yonghun Lee,[1] Caolan John,[1] Paul M. Neves,[1] S. Y. Frank Zhao,[1] Jonathan Denlinger,[5] Chris Jozwiak,[5] Aaron Bostwick,[5] Eli Rotenberg,[5] Efthimios Kaxiras,[6,7] David C. Bell,[7,8] Oleg Janson,[4] Riccardo Comin,[1] and Joseph G. Checkelsky[1,†]

[1]*Department of Physics, Massachusetts Institute of Technology, Cambridge, MA 02139, USA*

[2]*Department of Physics and Astronomy, Rutgers University, Piscataway, NJ 08854, USA*

[3]*Institute for Solid State Physics, TU Wien, 1040 Vienna, Austria*

[4]*Institute for Theoretical Solid State Physics, Leibniz IFW Dresden, 01069 Dresden, Germany*

[5]*Advanced Light Source, Lawrence Berkeley National Laboratory, Berkeley, CA 94720, USA*

[6]*Department of Physics, Harvard University, Cambridge, MA 02138, USA*

[7]*Harvard John A. Paulson School of Engineering and Applied Sciences, Harvard University, Cambridge MA 02138*

[8]*Center for Nanoscale systems, Harvard University, Cambridge, MA 02138, USA*

(Dated: November 29, 2023)

The introduction of localized electronic states into a metal can alter its physical properties, for example enabling exotic metal physics including heavy fermion and strange metal behavior. A common source of localized states in such systems are partially filled $4f$ and $5f$ shells because of the inherently compact nature of those orbitals. The interaction of electrons in these orbitals with the conduction sea is well described by the Kondo framework. However, there have also been observations of Kondo-like behavior in $3d$ transition metal oxides and in $4d$ and $5d$-containing van der Waals heterostructures. This calls for a broader consideration of the physical requirements for Kondo systems. Here we show transport and thermodynamic hallmarks of heavy fermion and strange metal behavior that arise in kagome metal Ni_3In, wherein the source of localized states is destructive interference-induced band flattening of partially filled Ni $3d$ states. With magnetic field and pressure tuning, we also find evidence that the system is proximate to quantum criticality, extending the analogy to f-electron Kondo lattices. These observations highlight the role of hopping frustration in metallic systems as a potential source for strong correlations. Additionally, this suggests a lattice-driven approach to realizing correlated metals with non-trivial band topology.

Landau Fermi liquid theory is successful in describing interacting fermions in a wide variety of metals [1]. Viewed intuitively as describing systems in which the charge carrying quasiparticles can be adiabatically connected to weakly interacting electrons in a Fermi gas [2], it explains the surprising validity of the single electron picture of metals often observed in complex, interacting materials. A celebrated case of this is conduction electrons interacting with a lattice arrary of localized magnetic moments (see Fig. 1(a)) [3, 4], which (via Kondo coherence) can result in a non-magnetic, renormalized Fermi liquid (schematically shown in Fig. 1(b)) consisting of well-defined fermionic quasiparticles with hundreds of times larger effective masses (*i.e.* heavy fermions) [5]. Another possible ground state for such a system is a metallic antiferromagnet in which Fermi liquid conduction electrons mediate the interaction between local magnetic moments. It is now well established that these two Fermi liquid phases are connected by a quantum critical point [6, 7] across which Fermi liquid

* Present Address: Division of Physics, Mathematics and Astronomy, California Institute of Technology, Pasadena, CA 91125, USA

† checkelsky@mit.edu

behavior can be disrupted. Therein the quasiparticles no longer resemble free electrons (schematically shown in Fig. 1(c)), but the system remains a conductor referred to as a strange metal [8]. Such behavior has attracted interest both for its enigmatic microscopic origin [8] and (in addition to quantum critical Kondo systems) its appearance in the normal state of high temperature superconductors [9] and, more recently, superconducting moiré heterostrucures [10]. The broadening of platforms for strange metal behavior offers an opportunity to examine its material requirements and potential insight into its underlying mechanisms.

Here we study the appearance of heavy fermion and strange metal behavior in intermetallic kagome metals. These materials have attracted significant recent interest for their ability to host unusual topological [11–14], superconducting [15], and magnetic [11–13] phases. A striking aspect of these systems is the connection between these phases and the model expectations of the underlying trihexagonal lattice, observed as Dirac [13], van Hove [16], and flat band states [14, 17]. The last among these draws connections to long-standing theoretical models for correlated electron physics based on destructive quantum interference [18]. However, realization of ideal flat bands in kagome metals faces several challenges, including departure from the model lattice due to hopping beyond nearest neighbor and orbital effects [14] and their stabilization at the Fermi level E_F [17]. While the condition for band flatness and its isolation from other bands at the Fermi level is particularly strict for generating *e.g.* gapped fractional topological phases [19], in this work we show that correlated metallic phases driven by a high degree of electronic degeneracy can be realized in kagome metals when narrow or partially flat bands are brought to E_F.

The transition metal intermetallic Ni_3In is a candidate for a kagome metal addressing the above criteria for a correlated metal. Crystallizing in space group $P6_3/mmc$, its basic structural unit is a breathing Ni kagome network which circumscribes In in the hexagonal void (see Fig. 1(d), these layers are AB stacked within a unit cell [20]). Density functional theory (DFT) calculations (see Fig. 1(e)) indicate a partially flat band within the Γ-M-K-Γ plane at E_F. In Fig. 1(f) we illustrate this dispersion, which exhibits a $k_z = 0$ bandwidth $W_0 \sim 60$ meV. With the expected Coulomb repulsion strength $U \sim 1$ eV as for elemental nickel [21], this implies $U \gg W_0$ for a significant density of states (DOS) even before the effects of interaction are considered. Motivated by the potential for a subsequent localized character for these electrons [22], we here explore this partial flat band and its interaction

with the dispersive bands in the system in the context of a hopping interference-driven realization of the Kondo lattice (Fig. 1(a)).

We first examine the transport and thermodynamic properties of the metallic state of Ni_3In. The electrical resistivity in the kagome planes $\rho_{ab}(T)$ of Ni_3In at zero magnetic field is shown in Fig. 2(a). Upon cooling from $T = 300$ K, $\rho_{ab}(T)$ is characterized by a broad shoulder which below $T = 100$ K gives way to approximately T-linear behavior. This T-linear behavior is a significant deviation from conventional Fermi liquid behavior ($\alpha = 2$ where α is the resistivity exponent in $\rho(T) \sim T^{\alpha}$) [23] and bears a stark contrast to several structurally related kagome metals whose $\rho(T)$ flattens out below 50 K (in which, notably, there are no partial flat bands at E_F, see Supplementary Information Fig. S11). As shown in the inset of Fig. 2(a), only at $T < 1.5$ K $\equiv T_{FL}$ a response of the form $\rho_{ab}(T) = \rho_0 + AT^2$ is recovered. The coefficient A of Ni_3In (0.25 $\mu\Omega$·cm·K^{-2}) is significantly larger than the upper bound estimated for the isostructural Ni_3Sn (1×10^{-4} $\mu\Omega$·cm·K^{-2}), indicating a strongly-enhanced electron-electron scattering in Ni_3In.

Turning to heat capacity C_p, we show C_p normalized by temperature C_pT^{-1} versus T^2 of Ni_3In in Fig. 2(b). At low-T an upturn is observed, deviating from the form $\gamma+\beta T^2$ expected for a Fermi liquid (γ is the Sommerfeld coefficient and βT^2 the phonon contribution). This becomes discernible at lower T than in electrical transport, recalling similar phenomenology reported in *e.g.* transition metal oxides [24, 25]. Also shown is the conventional Fermi liquid response for Ni_3Sn which according to DFT exhibits a similar electronic structure apart from an overall energy shift of approximately 0.25 eV (see Fig. 2(b) inset). Using the acoustic phonon contribution of Ni_3Sn (see dashed line in Fig. 2(b)), for Ni_3In we estimate $\gamma = 51.6$ mJ·K^{-2}·mol^{-1}, an approximately five-fold increase from 9 mJ·K^{-2}·mol^{-1} for Ni_3Sn. From γ we infer a density of states $\mathcal{D}(E_F) = 44$ eV^{-1} u.c.$^{-1}$ for Ni_3In, approximately three times that estimated from DFT (14 eV^{-1} u.c.$^{-1}$); in contrast, $\mathcal{D}(E_F)$ inferred from γ (7.6 eV^{-1} u.c.$^{-1}$) is only 50% larger than that expected from DFT (4.9 eV^{-1} u.c.$^{-1}$) for Ni_3Sn. The comparison signifies considerable renormalization and correlation effects driven by the placement (before interactions) of the flat electronic states at E_F in Ni_3In. Contrasting the low temperature A coefficient and γ additionally reveals the unusual nature of the metallic state realized in Ni_3In. This metallic state is marked by an extremely large Kadowaki-Woods ratio A/γ^2 as is shown in Fig. 2(c): $A_{ab}/\gamma^2 = 91$ $\mu\Omega$ cm mol^2 K^2 J^{-2} [26, 27], indicating an unconventional scattering process taking place within the kagome lattice plane. We note that

the Kadowaki-Woods ratio observed in our system is three orders of magnitude larger than those of elemental transition metals and lies closer to heavy fermion metals and correlated oxides, indicating an enhanced correlation in the electronic states of Ni_3In.

To shed additional light on the nature of the correlated metallic state in Ni_3In, we applied magnetic field and hydrostatic pressure as external tuning parameters to the system. In Fig. 3(a) we show high resolution measurements of $\rho_{ab}(T, H)$ of Ni_3In (see Fig. 3(a)). The evolution of the metallic state in Ni_3In can be seen most clearly in a map of $\alpha(T, H)$ in Fig. 3(b), the blue/green region ($\alpha = 0.9 \sim 1$) near $H = 0$ highlights a weak sublinear behavior of ρ_{ab}. Increasing H tends to suppress the (sub-)linearity and drive the system towards a Fermi liquid state at low T. Quantitatively, this is reflected in a systematic decrease of A and increase of T_{FL} with H (see Fig. 3(b) and Supplementary Information Fig. S14 and S15). The suppression of the zero-field non-Fermi liquid phase is also corroborated by C_p/T at fields (Fig. 3(a) inset). Applying a hydrostatic pressure (Fig. 3(c)) reveals a similar evolution of $\alpha(T, P)$ where pressure, like magnetic field, is found to suppress the non-Fermi liquid behavior. We hypothesize that the observed crossover between NFL and FL states with T and magnetic field, pressure, and doping (see Supplementary Information Fig. S23) arises from a phase space depicted in Fig. 4(a) wherein fluctuations from a nearby ordered phase serve as source of scattering tuned by the parameters δ. Such tunability is commonly observed in correlated electron systems with competing underlying energy scales [28], with the critical behavior being described as a strange metal, often showing a T-linear behavior over the temperature scale of associated quantum fluctuations. Notably, the overall resistivity of Ni_3In here up to room temperature (Fig. 2(a)) is qualitatively similar to that of heavy fermion metal $CeCu_{5.9}Au_{0.1}$ at an antiferromagnetic quantum critical point up to 1 K [29], and to that of optimally doped $BaFe_2(As_{1-x}P_x)_2$ up to 800 K [30]; the apparent common phenomenology despite the drastic difference in underlying materials and temperature scales is striking. While the multiband nature of the present system makes further quantifying the observed responses challenging, further experiments to probe potentially nearby quantum phase transitions and associated Fermi surface changes are crucial for further comparison with the broader class of strange metal systems [8].

Viewing the observed correlated metallic behavior with the DFT electronic structure with flattened bands at E_F (Fig. 1(d)), we propose the behavior of Ni_3In can be viewed as an emergent analogue of heavy fermion systems, comprised of coexisting localized magnetic

moments with the conduction electron sea (see schematic in Fig. 4(b)). A natural source of such magnetic moments are the partial flat band states; at high T these moments are weakly correlated, evidenced by a Curie-Weiss temperature dependence in the observed magnetic susceptibility χ as well as an onset of H-suppression of fluctuations in magnetoresistance (see Supplementary Information Fig. S13). Below approximately 80 K, short range correlations between the moments develop, leading to a growth of $\chi(T)$ deviating from a mean field Curie-Weiss form, and intense scattering of the conduction electrons including an approximate T-linear (strange metal) behavior for $\rho_{ab}(T)$, defining a NFL regime in Fig. 4(a,b). Finally, for $T < 1$ K a heavily renormalized metallic state appears marked by strongly enhanced scattering in the kagome plane.

Whereas the conventional starting point for modeling of heavy fermion systems is a localized moment interacting with a conduction electron sea, in the present case we hypothesize that both of these constituent elements arise from band features. In the following we discuss potential origin of the former from a band-theoretical perspective. The flat electronic states near E_F are found to be composed of d_{xz} orbitals in locally rotated coordinates; using an effective band model aimed to capture these states, we performed local $\chi_{\rm loc}$ and momentum-resolved magnetic susceptibility $\chi(\boldsymbol{q})$ calculations (see Supplementary Information Section SIII). A pronounced Curie-Weiss-like increase of $\chi_{\rm loc}$ with lowering T in the absence of correlation indicates a pre-formation of local moments [21] (see Supplementary Information Fig. S7). Additionally, $\chi(\boldsymbol{q})$ exhibits negligible momentum-dependence in the kagome plane (Fig. 4(c)); the the presence of an extended "hot region" across the kagome plane suggests that the magnetic instability of the partially filled flat band is of localized nature (Fig. 4(d)), distinct from prototypical itinerant magnetic orders driven by "hot spots" in momentum space (Fig. 4(e)) [31].

The above analysis supports the formation of local moments in the system when correlation is further introduced [21]; upon the formation of local moments, the lower energy physics is then dominated by how the array of local moments interact with the conduction electrons in the system, akin to heavy fermion and non-Fermi liquid behaviors observed in Kondo lattice systems [23]. We note that the observed pressure and field-driven crossover between NFL and FL is consistent with this picture: in the context of the Doniach phase diagram [4], pressure is expected to favor a screened heavy fermion liquid phase by increasing J, while magnetic field is found to favor a Fermi liquid phase as a result of suppression

of magnetic fluctuations in a variety of Kondo lattice quantum critical systems [29, 32]. The present system therefore establishes a distinct route to heavy fermion and associated quantum criticality from a pure band origin, potentially connecting to recent theoretical proposals for flat-band-driven Kondo behavior with elevated energy scales [33].

Tuning Ni_3In across a potential quantum phase transition into an ordered state as illustrated in the hypothetical phase diagram in Fig. 4(a) should help shed further light on the interaction between the conduction electron and the flat band electrons and put further constrains on theoretical models that can capture the low energy physics, particularly the non-Fermi liquid/strange metal behavior. Although it is found that neither magnetic field nor pressure can induce an ordered phase, future experimental exploration of the phase space spanned by additional non-thermal tuning parameters such as uniaxial stress, negative chemical pressure, or carrier doping are important to clarify the nature of potentially nearby magnetic and electronic instabilities. The breathing kagome lattice in Ni_3In itself in the context of antiferromagnetic interaction may lead to strong geometric frustration and emergent spin excitations relevant to understanding the present strange metal behavior [34, 35]. We note that Ni_3In also hosts a mirror-protected nodal ring near E_F (see Fig. 1(d) and Supplementary Information Fig. S2), providing a unique platform where topological electronic features may interact with a non-Fermi liquid state at E_F. It is also of significant future theoretical interest to compare the observed non-Fermi liquid behaviors in the present system with structurally related CoSn–which hosts flat bands with different dimensionality and/or orbital characters with the present system–as the Fermi level is tuned through the flat bands therein [14, 36].

The key design aspect here to realizing the unusual metallic states in Ni_3In lies in the frustration of hopping of the states at E_F from an cooperative destructive interference between lattice and orbital degrees of freedom. Our approach exemplifies an increased role of designing correlated systems from a non-interacting starting point, and in the meantime leverages the broad notion of using $3d$ electrons to increase interaction effects [37]. This suggests potential new insights into the behavior of previously reported d-electron heavy fermion systems which arise from frustrated networks (*e.g.* the V pyrochlore containing system LiV_2O_4 [38]) and van der Waals heterostructures [39, 40], and more broadly, a design paradigm for realizing correlated topological states [41]. Additionally, despite this significant departure from the design paradigm of f-electron [5], the resulting transport and quantum critical

phenomenology is strikingly similar. Common among these systems is the realization of significantly flattened electronic dispersion near the Fermi level, raising the possibility that the unifying driver for heavy fermion and strange metal behavior therein is "flat band" metallic states [33, 42, 43]. Such a broadened range of systems represents a vastly differentiated material landscape for examining theories of strongly correlated gapless phases.

A. Acknowledgments

We appreciate fruitful discussions with T. Senthil, B.J. Yang, L. Zou, Y. Zhang, K. Haule, J.-S. You, J. van den Brink, O.I. Motrunich, S. Bühler-Paschen, Q. Si, C. Varma, and M. Kriener. L.Y. acknowledges the assistance from M.K. Chan for pulsed field magnetization measurements. D.C.B. acknowledges the help of A. Akey for TEM sample preparation. This research is funded in part by the Gordon and Betty Moore Foundation EPiQS Initiative, through Grants GBMF3848 and GBMF9070 to J.G.C. (material synthesis), NSF grant DMR-1554891 (material design), ARO Grant No. W911NF-16-1-0034 (technique development), and the Air Force Office of Scientific Research (AFOSR) under award FA9550-22-1-0432 (advanced material analysis). L.Y., M.K. and E.K. acknowledge support by the STC Center for Integrated Quantum Materials, NSF grant number DMR-1231319. L.Y. acknowledges the Heising-Simons Physics Research Fellow Program and the Tsinghua Education Foundation. S.F. is partially supported by a Rutgers Center for Material Theory Distinguished Postdoctoral Fellowship. M.K. acknowledges support from the Samsung Scholarship from the Samsung Foundation of Culture. R.C. acknowledges support from the Alfred P. Sloan Foundation. O.J. was supported by the Leibniz Association through the Leibniz Competition. A portion of this work was performed at the National High Magnetic Field Laboratory, which is supported by the National Science Foundation Cooperative Agreement no. DMR-1644779, the State of Florida and the DOE. Pulsed magnetic field measurements at Los Alamos National Laboratory were supported by the U.S. Department of Energy BES Science at 100T grant. This research used the resources of the Advanced Light Source, a US Department of Energy (DOE) Office of Science User Facility under contract no. DE-AC02-05CH11231. The computations in this paper were run on the ITF/IFW computer clusters (Dresden, Germany) the FASRC Cannon cluster supported by the FAS Division

of Science Research Computing Group at Harvard University. We thank U. Nitzsche for technical assistance in maintaining computing resources at IFW Dresden. This work was performed in part at the Aspen Center for Physics, which is supported by National Science Foundation grant PHY-1607611.

B. Author Contribution

L.Y. and J.G.C. designed the study. L.Y. synthesized and characterized the single crystalline and polycrystalline materials, and performed and analyzed the physical property measurements, with assistance from C.J. (hydrostatic pressure measurements), P.M.N. (field rotation measurements), and S.Y.F.Z. (low temperature measurements). S.F., J. K., O.J. and E.K. performed the first principle analysis. M.K., Y.L., R.C. performed the photoemission experiments and analysis with the assistance of J.D., C.J., A.B., and E.R.; J.D. guided the process of sample surface preparation. D.C.B. performed the transmission electron microscopy measurements. L.Y. and J.G.C. wrote the manuscript with input from all the other authors.

C. Competing Interests Statement

The authors declare no competing interests.

D. Figure Captions

Fig. 1 — Flat band-induced emergent phases, and the partial flat band in Ni_3In (a) Schematic of a Kondo lattice composed of localized electrons and conduction electrons (c-electron). The localized electrons may come from f-electrons or flat bands. The gray traces illustrate the itinerancy of the conduction electrons. The Kondo lattice provides an avenue for (b) renomarlized (heavy) Fermi liquids and (c) non-Fermi liquid states. (d) Top view of the Ni_3In kagome layer in the ab plane. Green and gray atoms represent nickel and indium, respectively. (e) Density functional theory (DFT) band structure of Ni_3In without spin-orbit coupling. The high symmetry points and lines in the Brillouin zone are highlighted in (e) inset. (f) A magnified view of the partial flat band within $k_z = 0$ plane

illustrated along with the Fermi level E_F.

Fig. 2 — Non-Fermi liquid behavior and strong electron-electron scattering in Ni_3In (a) Resistivity ρ of isostructural Ni_3In (red) and Ni_3Sn (blue) as a function of temperature T in the kagome lattice plane. The inset shows ρ of Ni_3In down to 0.3 K where a Fermi liquid behavior is observed below 1.5 K. The black solid curve shows a T^2 fit to $\rho(T)$. (b) Heat capacity normalized by temperature $C_p \cdot T^{-1}$ of Ni_3In (red symbols) and Ni_3Sn (blue symbols) with respect to T^2. The black dashed line is an estimate of the Fermi liquid $C_p \cdot T^{-1}$ of Ni_3In and its slope is taken from a linear fit to $C_p \cdot T^{-1}$ over T^2 for Ni_3Sn below 80 K^2. Inset shows the relative electron filling of Ni_3In and Ni_3Sn in a rigid band model. (c) Kadowaki-Woods ratio A/γ^2 of Ni_3In in comparison with various strongly correlated electron systems in an A-γ diagram adapted from Ref. [26].

Fig. 3 — Tuning the non-Fermi liquid (NFL)-Fermi liquid (FL) crossover in Ni_3In (a) In-plane resistivity ρ_{ab} below 25 K at various applied magnetic fields along the c-axis. Inset shows heat capacity without magnetic field (red symbols) and with an applied field of 9 T (black symbols). (b,c) Resistivity power α in the T-H (b) and T-P (c) phase spaces, respectively. α is calculated from $d\ln(\rho - \rho_0)/d\ln T$ with ρ_0 the extrapolated zero temperature limit of ρ.

Fig. 4 — The correlated metallic state and flat band-induced magnetic fluctuations in Ni_3In (a) Hypothetical quantum critical phase diagram with external tuning parameter δ. The thick gradient line shows the proposed location of Ni_3In at zero field and ambient pressure. The gray shaded area illustrates the parameter space traversed by magnetic field, pressure, and Sn-doping. (b) Schematics of the metallic phases realized in Ni_3In in different temperature regimes: above 80 K the system can be viewed as weakly-correlated local moments embedded in a conduction electron sea; below 80 K a non-Fermi liquid phase is realized showing a T-linear behavior in $\rho(T)$; below 1 K a correlated Fermi liquid phase is realized. (c) Momentum-dependent susceptibility $\chi(\boldsymbol{q})$ of the flat band in the $q_z = 0$ plane. The color scale of $\chi(q)$ is shown on the right. (d,e) Schematics of $\chi(\boldsymbol{q})$ for localized (d) and itinerant (e) magnetic fluctuations.

---

[1] G. Baym and C. Pethick, *Landau Fermi-liquid theory: concepts and applications* (John Wiley & Sons, 2008).

[2] P. W. Anderson, *Basic notions of condensed matter physics* (CRC Press, 2018).

[3] J. Kondo, Resistance minimum in dilute magnetic alloys, Progress of theoretical physics **32**, 37 (1964).

[4] S. Doniach, The kondo lattice and weak antiferromagnetism, physica B+ C **91**, 231 (1977).

[5] P. Coleman, Heavy fermions: electrons at the edge of magnetism, in *Handbook of Magnetism and Advanced Magnetic Materials*, edited by H. Kronmuller and S. Parkin (John Wiley and Sons, 2007) pp. 95–148.

[6] P. Gegenwart, Q. Si, and F. Steglich, Quantum criticality in heavy-fermion metals, nature physics **4**, 186 (2008).

[7] Q. Si and F. Steglich, Heavy fermions and quantum phase transitions, Science **329**, 1161 (2010).

[8] P. W. Phillips, N. E. Hussey, and P. Abbamonte, Stranger than metals, Science **377**, eabh4273 (2022).

[9] C. Proust and L. Taillefer, The remarkable underlying ground states of cuprate superconductors, Annual Review of Condensed Matter Physics **10**, 409 (2019).

[10] A. Jaoui, I. Das, G. Di Battista, J. Díez-Mérida, X. Lu, K. Watanabe, T. Taniguchi, H. Ishizuka, L. Levitov, and D. K. Efetov, Quantum critical behaviour in magic-angle twisted bilayer graphene, Nature Physics **18**, 633 (2022).

[11] A. K. Nayak, J. E. Fischer, Y. Sun, B. Yan, J. Karel, A. C. Komarek, C. Shekhar, N. Kumar, W. Schnelle, J. Kübler, *et al.*, Large anomalous hall effect driven by a nonvanishing berry curvature in the noncolinear antiferromagnet Mn_3Ge, Science advances **2**, e1501870 (2016).

[12] S. Nakatsuji, N. Kiyohara, and T. Higo, Large anomalous hall effect in a non-collinear antiferromagnet at room temperature, Nature **527**, 212 (2015).

[13] L. Ye, M. Kang, J. Liu, F. Von Cube, C. R. Wicker, T. Suzuki, C. Jozwiak, A. Bostwick, E. Rotenberg, D. C. Bell, *et al.*, Massive dirac fermions in a ferromagnetic kagome metal, Nature **555**, 638 (2018).

[14] M. Kang, S. Fang, L. Ye, H. C. Po, J. Denlinger, C. Jozwiak, A. Bostwick, E. Rotenberg, E. Kaxiras, J. G. Checkelsky, *et al.*, Topological flat bands in frustrated kagome lattice CoSn, Nature communications **11**, 4004 (2020).

[15] B. R. Ortiz, S. M. Teicher, Y. Hu, J. L. Zuo, P. M. Sarte, E. C. Schueller, A. M. Abeykoon, M. J. Krogstad, S. Rosenkranz, R. Osborn, *et al.*, CsV_3Sb_5: A z_2 topological kagome metal

with a superconducting ground state, Physical Review Letters **125**, 247002 (2020).

[16] M. Kang, S. Fang, J.-K. Kim, B. R. Ortiz, S. H. Ryu, J. Kim, J. Yoo, G. Sangiovanni, D. Di Sante, B.-G. Park, *et al.*, Twofold van hove singularity and origin of charge order in topological kagome superconductor CsV_3Sb_5, Nature Physics **18**, 301 (2022).

[17] M. Kang, L. Ye, S. Fang, J.-S. You, A. Levitan, M. Han, J. I. Facio, C. Jozwiak, A. Bostwick, E. Rotenberg, *et al.*, Dirac fermions and flat bands in the ideal kagome metal FeSn, Nature materials **19**, 163 (2020).

[18] D. L. Bergman, C. Wu, and L. Balents, Band touching from real-space topology in frustrated hopping models, Physical Review B **78**, 125104 (2008).

[19] E. Tang, J.-W. Mei, and X.-G. Wen, High-temperature fractional quantum hall states, Physical review letters **106**, 236802 (2011).

[20] R. Baranova, An electron diffraction study of the Ni−In system, SOVIET PHYS CRYSTALLOGR **10**, 24 (1965).

[21] A. Hausoel, M. Karolak, E. Şaşıoğlu, A. Lichtenstein, K. Held, A. Katanin, A. Toschi, and G. Sangiovanni, Local magnetic moments in iron and nickel at ambient and earths core conditions, Nature communications **8**, 16062 (2017).

[22] A. Hausoel, M. Karolak, E. Şaşıoğlu, A. Lichtenstein, K. Held, A. Katanin, A. Toschi, and G. Sangiovanni, Local magnetic moments in iron and nickel at ambient and earths core conditions, Nature communications **8**, 16062 (2017).

[23] G. Stewart, Non-fermi-liquid behavior in d-and f-electron metals, Reviews of modern Physics **73**, 797 (2001).

[24] R. Daou, N. Doiron-Leyraud, D. LeBoeuf, S. Li, F. Laliberté, O. Cyr-Choiniere, Y. Jo, L. Balicas, J.-Q. Yan, J.-S. Zhou, *et al.*, Linear temperature dependence of resistivity and change in the fermi surface at the pseudogap critical point of a high-t_c superconductor, Nature Physics **5**, 31 (2009).

[25] B. Michon, C. Girod, S. Badoux, J. Kačmarčík, Q. Ma, M. Dragomir, H. Dabkowska, B. Gaulin, J.-S. Zhou, S. Pyon, *et al.*, Thermodynamic signatures of quantum criticality in cuprate superconductors, Nature **567**, 218 (2019).

[26] S. Li, L. Taillefer, D. Hawthorn, M. Tanatar, J. Paglione, M. Sutherland, R. Hill, C. Wang, and X. Chen, Giant electron-electron scattering in the fermi-liquid state of $Na_{0.7}CoO_2$, Physical review letters **93**, 056401 (2004).

[27] A. Jacko, J. Fjærestad, and B. Powell, A unified explanation of the Kadowaki–Woods ratio in strongly correlated metals, Nature Physics **5**, 422 (2009).

[28] E. Dagotto, Complexity in strongly correlated electronic systems, Science **309**, 257 (2005).

[29] H. v. Löhneysen, T. Pietrus, G. Portisch, H. Schlager, A. Schröder, M. Sieck, and T. Trappmann, Non-fermi-liquid behavior in a heavy-fermion alloy at a magnetic instability, Physical review letters **72**, 3262 (1994).

[30] D. Hu, H. Hu, W. Zhang, Y. Wei, S. Li, Y. Gu, X. Ma, D. L. Abernathy, S. Chi, T. J. Williams, *et al.*, {\omega}/t scaling and magnetic quantum criticality in $BaFe_2(As_{0.7}P_{0.3})_2$, arXiv preprint arXiv:1812.11902 (2018).

[31] T. Moriya, Recent progress in the theory of itinerant electron magnetism, Journal of Magnetism and Magnetic Materials **14**, 1 (1979).

[32] P. Coleman and A. H. Nevidomskyy, Frustration and the kondo effect in heavy fermion materials, Journal of Low Temperature Physics **161**, 182 (2010).

[33] L. Chen, F. Xie, S. Sur, H. Hu, S. Paschen, J. Cano, and Q. Si, Emergent flat band and topological kondo semimetal driven by orbital-selective correlations, arXiv preprint arXiv:2212.08017 (2022).

[34] O. I. Motrunich, Variational study of triangular lattice spin-1/2 model with ring exchanges and spin liquid state in κ-$(ET)_2Cu_2(CN)_3$, Physical Review B **72**, 045105 (2005).

[35] H. Zhao, J. Zhang, M. Lyu, S. Bachus, Y. Tokiwa, P. Gegenwart, S. Zhang, J. Cheng, Y.-f. Yang, G. Chen, *et al.*, Quantum-critical phase from frustrated magnetism in a strongly correlated metal, Nature Physics **15**, 1261 (2019).

[36] B. C. Sales, W. R. Meier, D. S. Parker, L. Yin, J. Yan, A. F. May, S. Calder, A. A. Aczel, Q. Zhang, H. Li, *et al.*, Chemical control of magnetism in the kagome metal $CoSn_{1-x}In_x$: Magnetic order from nonmagnetic substitutions, Chemistry of Materials **34**, 7069 (2022).

[37] J. Smith and E. Kmetko, Magnetism or bonding: A nearly periodic table of transition elements, Journal of the Less Common Metals **90**, 83 (1983).

[38] S. Kondo, D. Johnston, C. Swenson, F. Borsa, A. Mahajan, L. Miller, T. Gu, A. Goldman, M. Maple, D. Gajewski, *et al.*, LiV_2O_4: A heavy fermion transition metal oxide, Physical review letters **78**, 3729 (1997).

[39] V. Vaňo, M. Amini, S. C. Ganguli, G. Chen, J. L. Lado, S. Kezilebieke, and P. Liljeroth, Artificial heavy fermions in a van der waals heterostructure, Nature **599**, 582 (2021).

[40] W. Zhao, B. Shen, Z. Tao, Z. Han, K. Kang, K. Watanabe, T. Taniguchi, K. F. Mak, and J. Shan, Gate-tunable heavy fermions in a moir\'e kondo lattice, Nature **616**, 61 (2023).

[41] L. Chen, C. Setty, H. Hu, M. G. Vergniory, S. E. Grefe, L. Fischer, X. Yan, G. Eguchi, A. Prokofiev, S. Paschen, *et al.*, Topological semimetal driven by strong correlations and crystalline symmetry, Nature Physics **18**, 1341 (2022).

[42] Z.-D. Song and B. A. Bernevig, Magic-angle twisted bilayer graphene as a topological heavy fermion problem, Physical review letters **129**, 047601 (2022).

[43] N. Regnault, Y. Xu, M.-R. Li, D.-S. Ma, M. Jovanovic, A. Yazdani, S. S. Parkin, C. Felser, L. M. Schoop, N. P. Ong, *et al.*, Catalogue of flat-band stoichiometric materials, Nature **603**, 824 (2022).

[44] G. Kresse and J. Furthmüller, Efficient iterative schemes for ab initio total-energy calculations using a plane-wave basis set, Physical review B **54**, 11169 (1996).

[45] G. Kresse and J. Furthmüller, Efficiency of ab-initio total energy calculations for metals and semiconductors using a plane-wave basis set, Computational materials science **6**, 15 (1996).

[46] P. E. Blöchl, Projector augmented-wave method, Physical review B **50**, 17953 (1994).

[47] J. P. Perdew, K. Burke, and M. Ernzerhof, Generalized gradient approximation made simple, Physical review letters **77**, 3865 (1996).

[48] A. A. Mostofi, J. R. Yates, Y.-S. Lee, I. Souza, D. Vanderbilt, and N. Marzari, wannier90: A tool for obtaining maximally-localised wannier functions, Computer physics communications **178**, 685 (2008).

[49] A. A. Mostofi, J. R. Yates, G. Pizzi, Y.-S. Lee, I. Souza, D. Vanderbilt, and N. Marzari, An updated version of wannier90: A tool for obtaining maximally-localised wannier functions, Computer Physics Communications **185**, 2309 (2014).

[50] N. Marzari, A. A. Mostofi, J. R. Yates, I. Souza, and D. Vanderbilt, Maximally localized wannier functions: Theory and applications, Reviews of Modern Physics **84**, 1419 (2012).

[51] K. Koepernik and H. Eschrig, Full-potential nonorthogonal local-orbital minimum-basis band-structure scheme, Physical Review B **59**, 1743 (1999).

[52] H. Eschrig and K. Koepernik, Tight-binding models for the iron-based superconductors, Physical Review B **80**, 104503 (2009).

METHODS

E. Materials Synthesis

Single crystals of Ni_3In were synthesized via an I_2-catalyzed reaction. The starting materials of Ni and In powders in 3:1 molar ratio were mixed with I_2 pieces and sealed in an evacuated quartz tube. The quartz tube was heated up to 800 °C and kept for more than two weeks. Hexagonal prism-shaped crystals (typical lateral size $300 \sim 500\mu$m) can be obtained and are found to be stable in air. Single crystals of Ni_3Sn were synthesized via chemical vapor transport. Ni powder and Sn pieces with 3:1 molar ratio were loaded into an evacuated quartz tube with the addition of $5mg/cm^3$ I_2. The growth took place at a temperature gradient from 850 °C to 700 °C for two weeks and the primary morphology of the crystals were needle-like. The phase of the crystals was confirmed with X-ray diffraction. The polycrystals of $Ni_3In_{1-x}Sn_x$ were synthesized by mixing the stoichiometric powder and kept in evacuated quartz tubes at 800 °C for 3-5 days. The product was ground to powder and the above process was repeated multiple times to improve homogeneity. The polycrystalline samples for heat capacity measurements are pelletized and sintered at 800 °C for 3-5 days. The scanning electron microscopy (SEM) images of single crystals were taken in a FEI Helios Nanolab 600 dual beam microscope.

F. Physical Properties Measurements

The electrical transport measurements were performed on single crystals and polycrystals with the standard five probe method in a commercial cryostat and also at the National High Magnetic Field Laboratory (NHMFL) DC field facility. We have used focused ion beam (FIB) to structure a thin piece of crystal (~ 5 μm thick) for transport measurements. The FIB fabrication was performed with a FEI Helios Nanolab 600 dual beam microscope with a Ga ion beam flux of 21 nA at the magnification of 350. Resistivity measurements under hydrostatic pressure were performed in an HPC-33 piston-type pressure cell (ElectroLab Corp.) with Daphne7373 as the pressure transmitting medium. The heat capacity measurements are performed on sintered polycrystals using the two relaxation time method. In-house magnetic susceptibility measurements are performed in the Vibrating Sample Magnetometer (VSM) with the Quantum Design Magnetic Property Measurement System (MPMS3).

Magnetization measurements up to 60 T were performed at the NHMFL Pulsed Field facility at the Los Alamos National Laboratory.

G. Scanning Transmission Electron Microscopy

Scanning Transmission Electron Microscopy (STEM) experiments were conducted on a JEOL ARM 200CFG probe corrected microscope at an accelerating voltage of 200 kV. Ni_3In samples were prepared by a Helios focused-ion beam (Thermo Electron) operated at an acceleration voltage of 30 kV for the gallium beam lift-out, followed by 1 keV final Argon polish with a (Fischione) Nanomill for 15 minutes.

H. Angle-resolved Photoemission Spectroscopy

Angle-resolved Photoemission Spectroscopy (ARPES) experiments were performed at the Beamline 7.0.2 (MAESTRO) of the Advanced Light Source. The experiments were conducted at the micro-ARPES endstation equipped with a R4000 hemispherical electron analyzer (Scienta Omicron). Ni_3In samples were not cleavable by standard post-cleaving procedure. We thus prepared the surface of Ni_3In by *ex situ* fine polishing followed by in situ Ar^+ ion-sputtering and annealing at 700 °C. Recovery of the Ni_3In surface structure after the sputter-annealing cycles were confirmed by *in situ* low-energy electron diffraction (LEED) feedback. The atomically flat surface of Ni_3Sn is prepared by standard *in-situ* low-temperature cleaving. ARPES measurements were conducted at the liquid nitrogen temperature ($\sim$ 80 K) and under the ultrahigh vacuum better than 4×10^{-11} torr. Photon energy-dependence was investigated over a wide energy range from 70 eV to 230 eV to identify high-symmetry positions along the k_z momentum-space directions. The high-symmetry points (Γ and Z) and periodicity along k_z were well-reproduced through the nearly-free-electron final state model with inner potential 10 eV. All spectra were collected with p-polarized photons. The energy and momentum resolutions were below 20 meV and 0.01 Å^{-1}, respectively.

I. First-principles Electronic Structure Calculation

The *ab initio* density functional theory (DFT) calculations were performed by Vienna Ab initio Simulation Package (VASP) [44, 45]. The pseudo potential formalism is based on the Projector augmented wave method (PAW) [46] with exchange-correlation energy parametrized by Perdew, Burke and Ernzerhof (PBE) [47], a functional of the generalized gradient approximation (GGA) type. The DFT calculations for the bulk Ni_3In crystal are converged with an energy cut-off 360 eV for the plane-wave basis and a $13 \times 13 \times 11$ Monkhorst-Pack grid sampling in the reciprocal space. To analyze the DFT electronic structure, we employed the Wannier90 code [48, 49] to construct Wannier tight-binding Hamiltonian [50], using the localized Wannier basis projected from Ni $3d$, $4s$ and In $5s$ states. The further simplified effective 6-band model projected from the locally rotated d_{xz} orbitals is also derived similarly.

To construct an effective model based on molecular rather than atomic orbitals, we additionally carried out DFT calculations using the full-potential local-orbital code FPLO [51] version 18. Its built-in module [52] allows the user to construct Wannier projections for molecular-like states comprising several atomic orbitals. Since the GGA orbital-resolved density of states (DOS) revealed the dominance of Ni d_{xy} and d_{xz} contributions in the vicinity of the Fermi level, we restricted ourselves to these atomic orbitals. Molecular orbitals were constructed by combining the respective orbitals of three Ni atoms forming a triangle on the kagome lattice. In this way, we obtained an effective model with two sites per cell and two orbitals per site, giving rise to four bands. To cross-check results magnetic susceptibilities calculated using different models, we also performed an automatic wannierization, which yields a model describing all valence states (excluding core and semi-core states).

With the effective model , we have evaluated the local magnetic susceptibility $\chi^0_{\rm loc}$, defined as

$$\chi^0_{\rm loc}(\omega=0) = -\frac{2\mu_{\rm B}^2}{\beta}\sum_{ij}\sum_{\omega_n} G^{0,\rm loc}_{ij}(\omega_n)G^{0,\rm loc}_{ji}(\omega_n), \tag{1}$$

with the Matsubara frequency ω_n and $G^{0,\rm loc}_{ij}(\omega_n) = \frac{1}{N_{\vec{k}}}\sum_{\vec{k}} G^0_{ij}(\vec{k},\omega_n)$. The Curie-Weiss-like temperature dependence $\chi^0_{\rm loc}$ for the Ni_3In effective model can be contrasted with a simple metal, modeled by a single-band three-dimensional cubic lattice with an energy dispersion $E = (\cos(k_x) + \cos(k_y)) + \cos(k_z))/3$. We calculated $\chi^0_{\rm loc}$ using a $24 \times 24 \times 24$ momentum

sampling grid with a 2 eV bandwidth and chemical potential at $E = 0.5$ eV,

J. Data Availability

The datasets for the main text are available in the Supplementary Information. All other data available from the corresponding author on reasonable request.

K. Code availability

The codes used to support the findings in this study are available from the corresponding author on reasonable request.

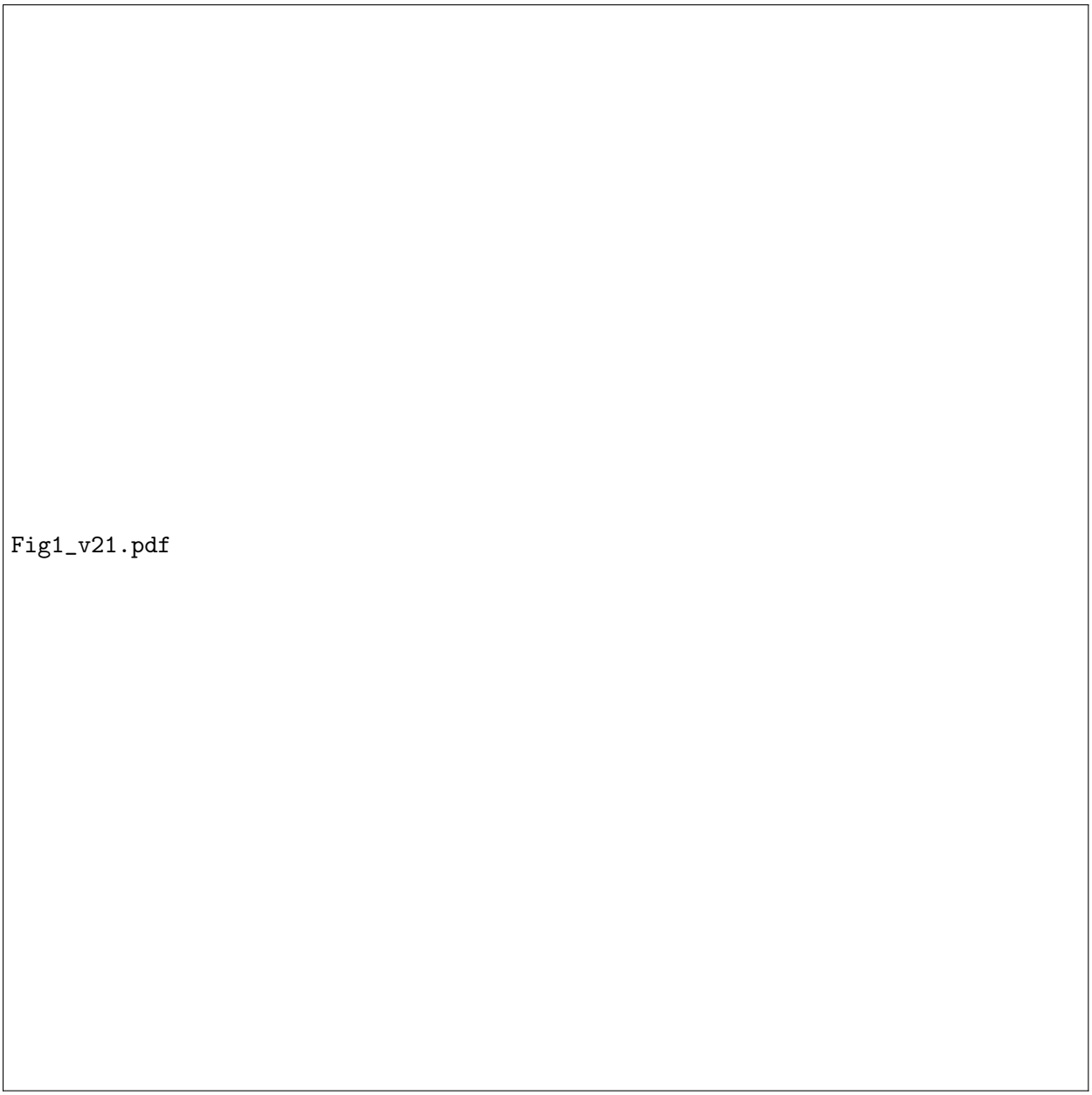

FIG. 1.

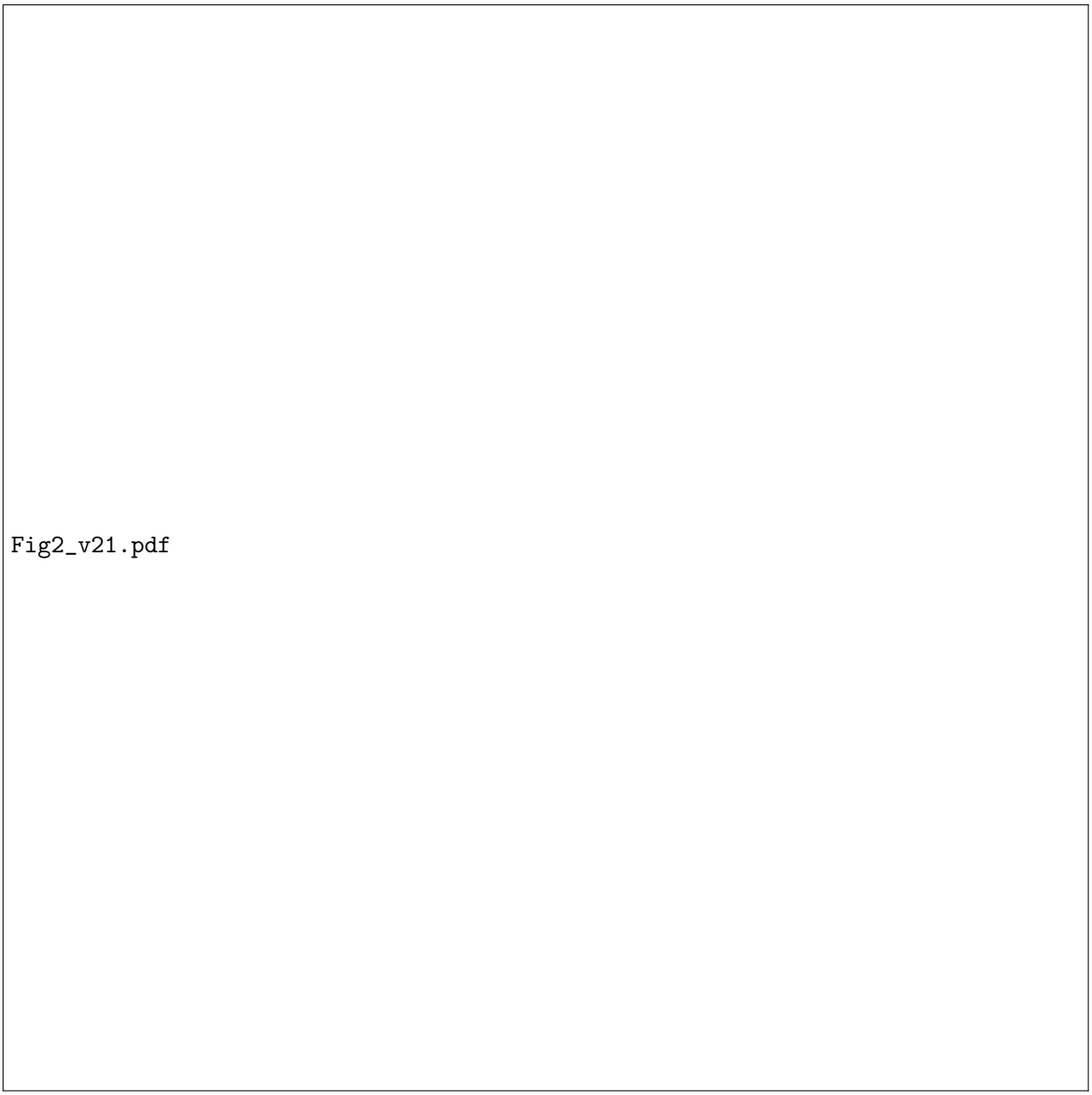

FIG. 2.

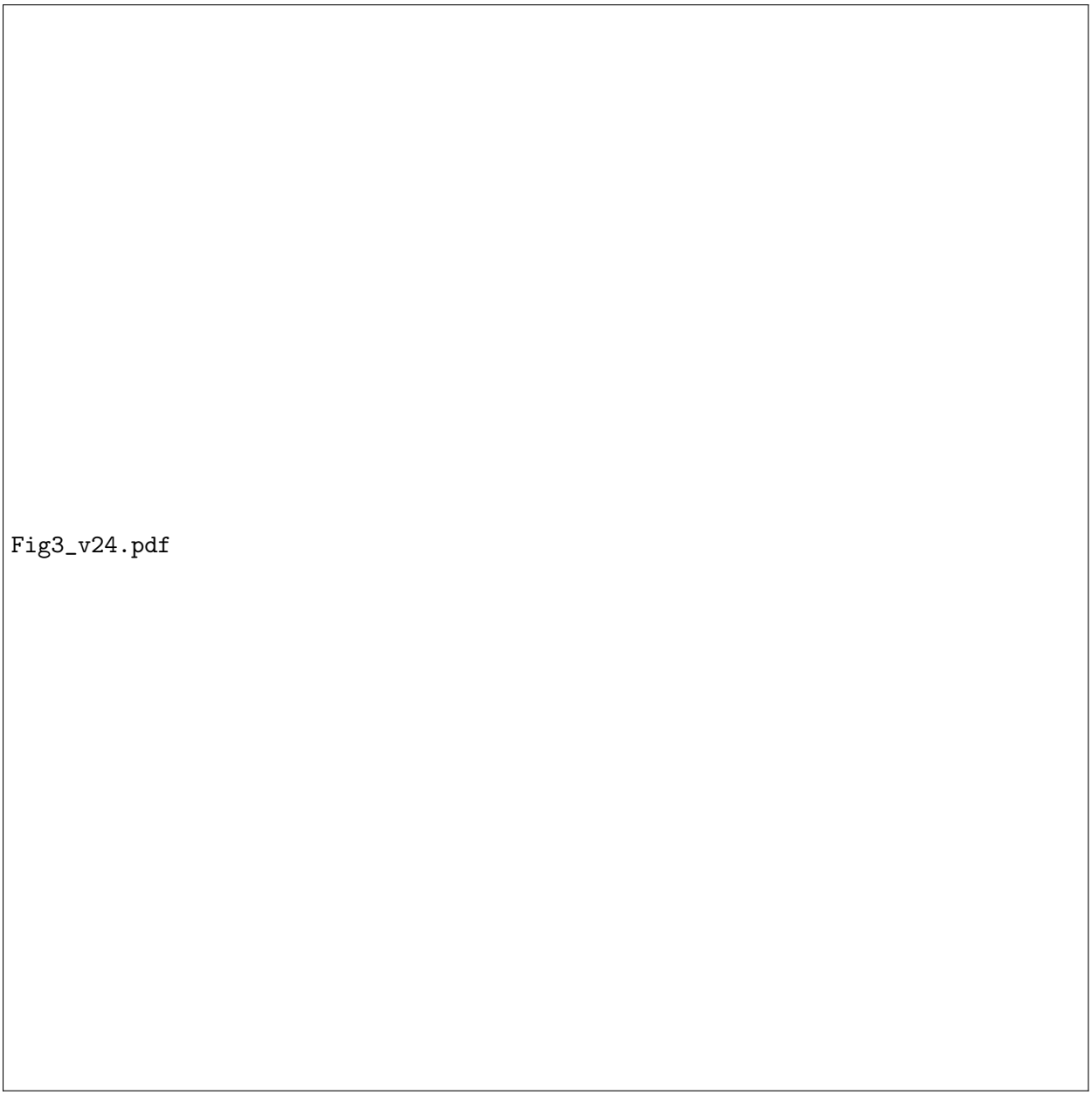

FIG. 3.

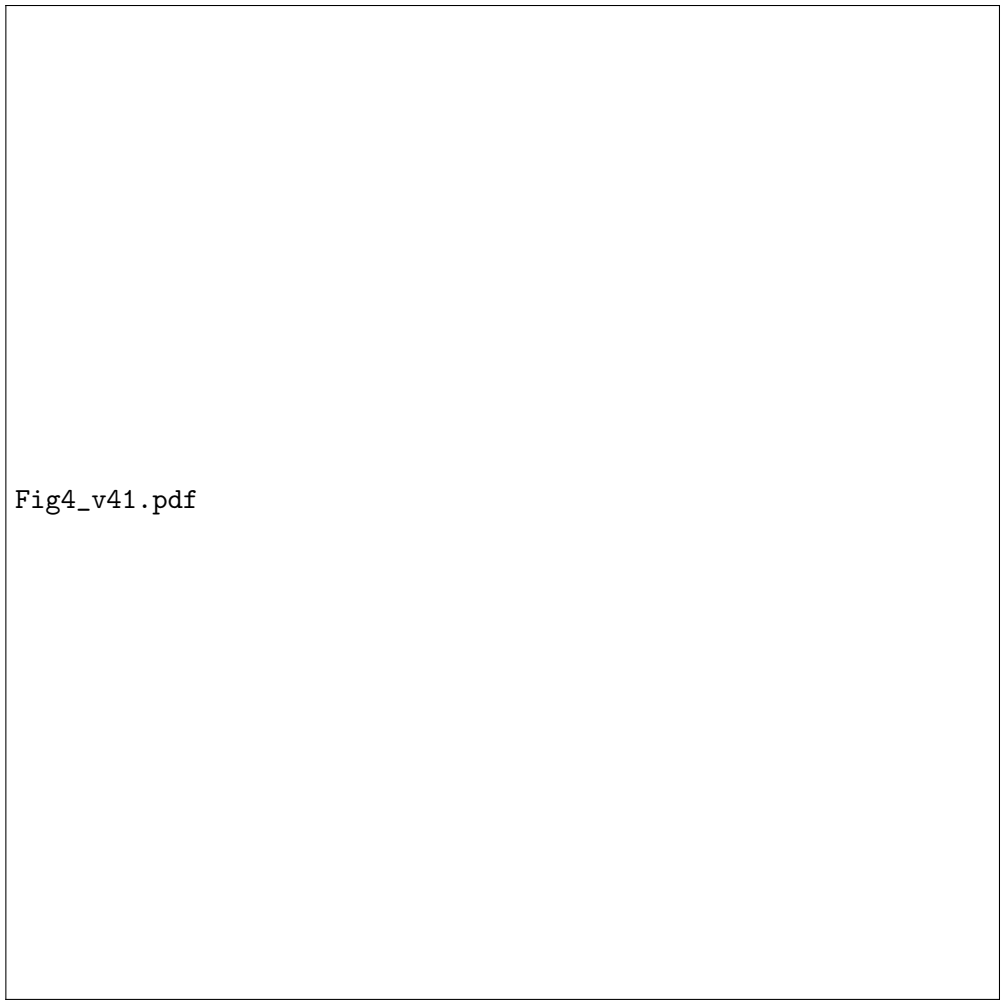

FIG. 4.

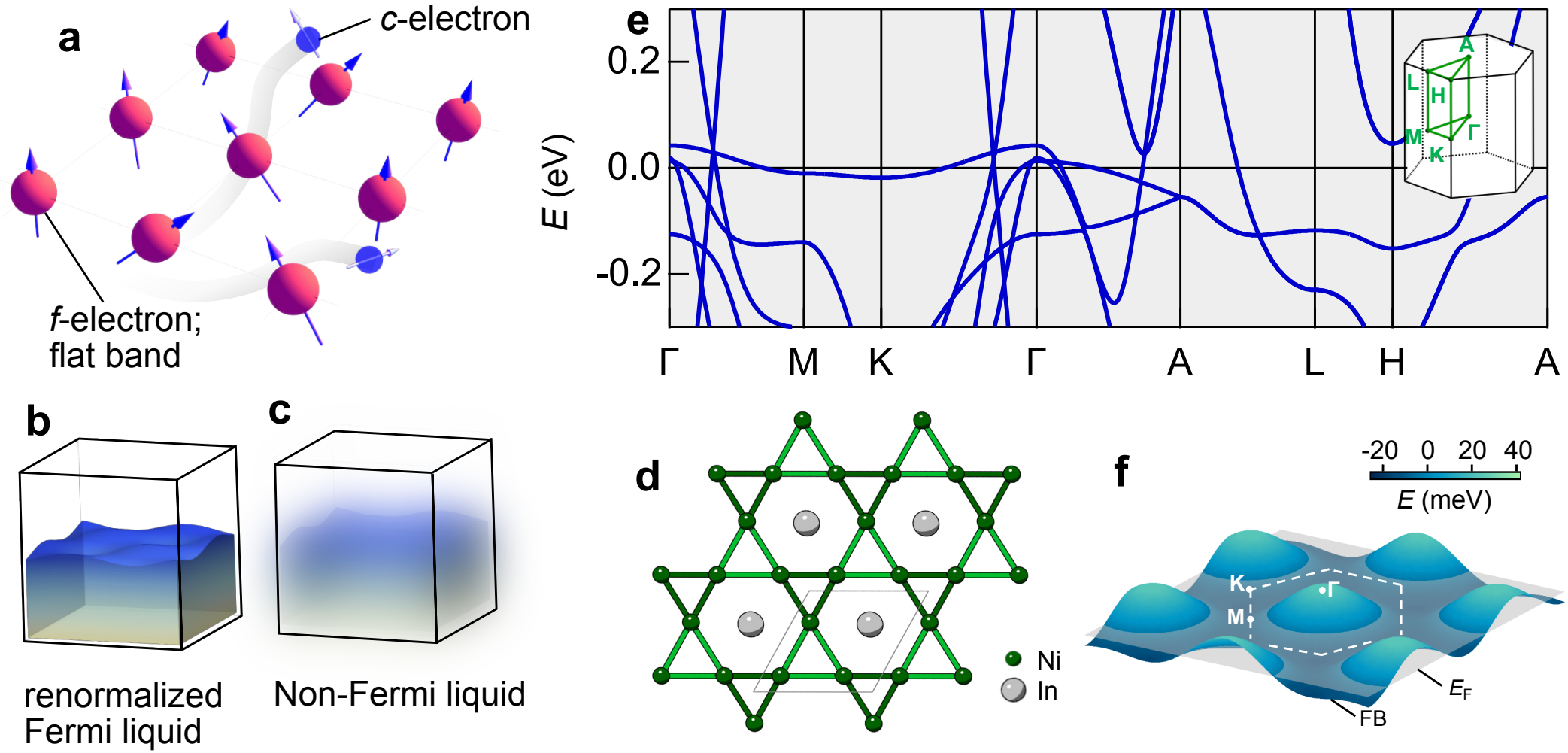
a
c-electron
f-electron;
flat band
e
0.2
0.0
-0.2
E (eV)
Γ
M
K
Γ
A
L
H
A
b
renormalized
Fermi liquid
c
Non-Fermi liquid
d
Ni
In
f
-20
0
20
40
E (meV)
K
M
Γ
E_F
FB

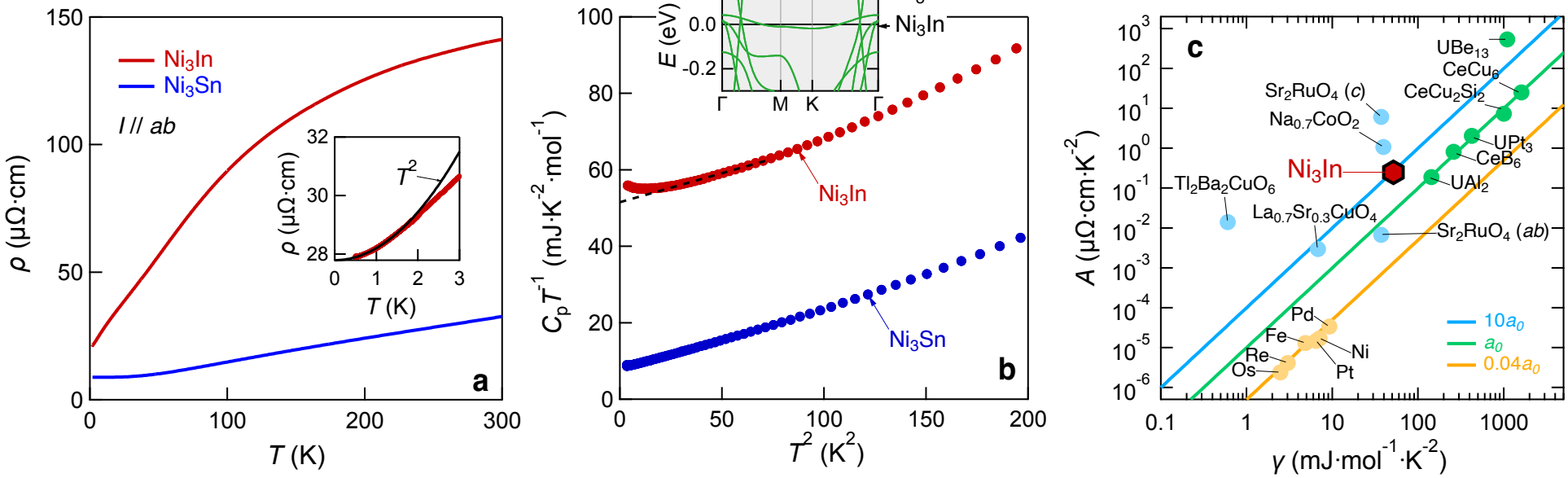
Ni3In
Ni3Sn
I // ab
ρ (μΩ·cm)
T (K)
T2
a
Ni3Sn
Ni3In
E (eV)
Γ M K Γ
CpT-1 (mJ·K-2·mol-1)
T2 (K2)
b
c
UBe13
CeCu6
Sr2RuO4 (c)
CeCu2Si2
Na0.7CoO2
UPt3
CeB6
Ni3In
UAl2
Tl2Ba2CuO6
La0.7Sr0.3CuO4
Sr2RuO4 (ab)
Pd
Fe
Re
Os
Ni
Pt
10a0
a0
0.04a0
A (μΩ·cm·K-2)
γ (mJ·mol-1·K-2)

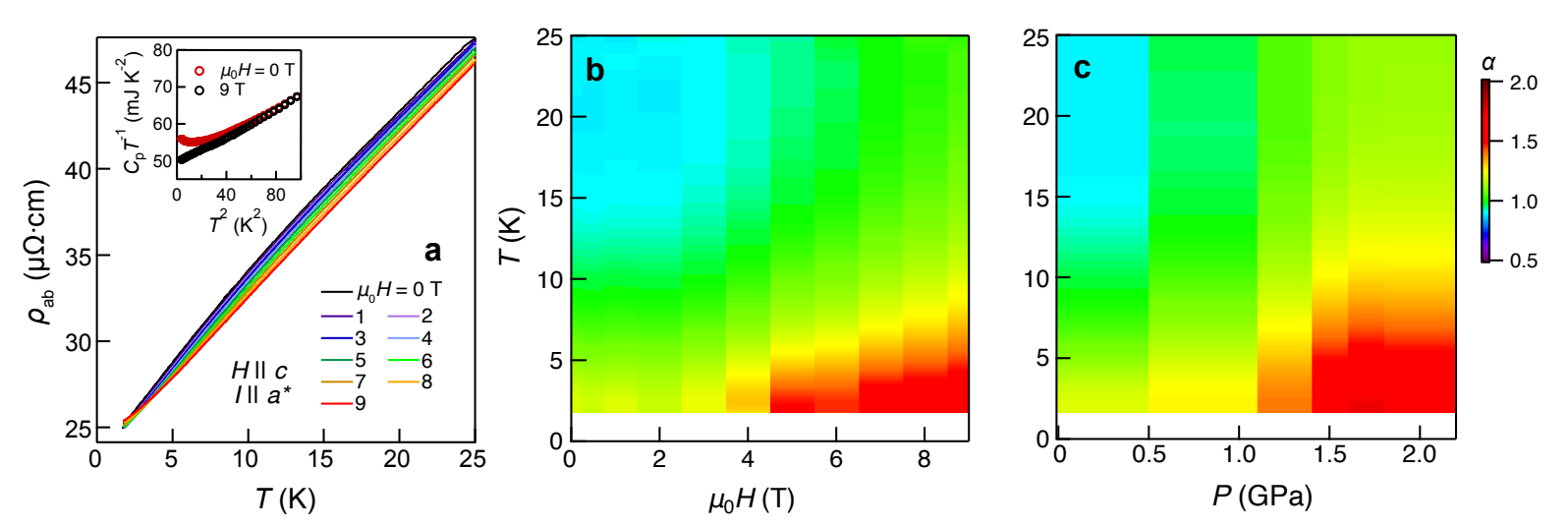
a
ρ_{ab} ($\mu\Omega$·cm)
T (K)
$H \parallel c$
$I \parallel a^*$
μ_0H = 0 T
1
2
3
4
5
6
7
8
9
C_pT^{-1} (mJ K^{-2})
T^2 (K^2)
μ_0H = 0 T
9 T
b
T (K)
μ_0H (T)
c
P (GPa)
α

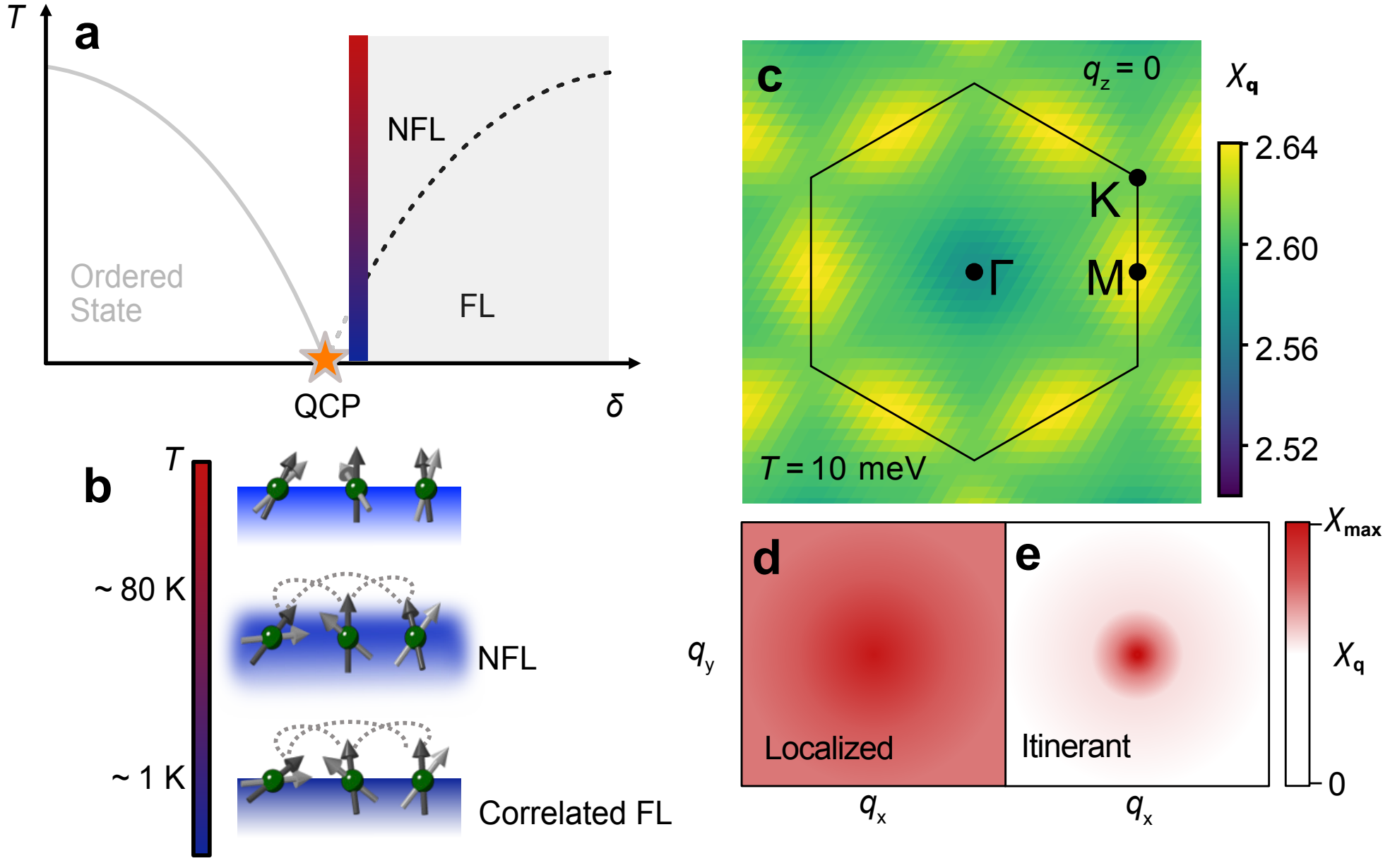
a
T
NFL
Ordered
State
FL
QCP
δ
b
T
~ 80 K
~ 1 K
NFL
Correlated FL
c
$q_z = 0$
χ_q
2.64
2.60
2.56
2.52
K
Γ
M
$T = 10$ meV
d
e
q_y
Localized
Itinerant
q_x
q_x
χ_{max}
χ_q
0